Biosensors and Bioelectronics 145 (2019) 111719

Contents lists available at ScienceDirect

Biosensors and Bioelectronics

journal homepage: http://www.elsevier.com/locate/bios

Dual-color magnetic-quantum dot nanobeads as versatile fluorescent probes in test strip for simultaneous point-of-care detection of free and complexed prostate-specific antigen

Zhen Rong [a,b,1], Zikun Bai [a,b,1], Jianing Li [a,b,1], Hao Tang [c], Tianyi Shen [c], Qiong Wang [a,d], Chongwen Wang [a,b,e,*], Rui Xiao [a,b,**], Shengqi Wang [a,b,***]

[a] Beijing Institute of Radiation Medicine, Beijing, 100850, PR China
[b] Beijing Key Laboratory of New Molecular Diagnosis Technologies for Infectious Diseases, Beijing, 100850, PR China
[c] Department of Urology, Nanjing Jinling Hospital, Nanjing, 210002, PR China
[d] Beijing Meiling Biotechnology Corporation, Beijing, 102600, PR China
[e] College of Life Sciences, Anhui Agricultural University, Hefei, 230036, PR China

ARTICLE INFO

Keywords:
Prostate cancer
Free and complexed prostate-specific antigen
Magnetic-quantum dot nanobead
Fluorescent lateral flow immunoassay
Simultaneous detection
Point-of-care

ABSTRACT

Simultaneous detection of free and complexed prostate-specific antigen (f-PSA and c-PSA) is critical to the prostate cancer (PCa) diagnostic accuracy for clinical samples with PSA values in the diagnostic gray zone between 4 and 10 ng mL^{-1}. Herein, red and green magnetic-quantum dot nanobeads (MQBs) with superior magnetic property and high luminescence were fabricated via polyethyleneimine-mediated electrostatic adsorption of numerous quantum dots onto superparamagnetic Fe_3O_4 magnetic cores, and were conjugated with f-PSA antibody and c-PSA antibody, respectively, as versatile fluorescent probes in test strip for immune recognition, magnetic enrichment, and simultaneous detection of f-PSA and c-PSA analytes in complex biological matrix with t-PSA antibody on the test line. A low-cost and portable smartphone readout device with an application was also developed for the imaging of dual-color test strips and data processing. This assay can simultaneously detect f-PSA and c-PSA with the limits of detection of 0.009 ng mL^{-1} and 0.087 ng mL^{-1}, respectively. Clinical serum samples of PCa and benign prostatic hyperplasia patients were evaluated to confirm the clinical feasibility. The results suggest that the proposed dual-color MQBs-based fluorescent lateral flow immunoassay is a promising point-of-care diagnostics technique for the accurate diagnosis of PCa even in resource-limited settings.

1. Introduction

Prostate cancer (PCa) is a common cancer among males in the United States with a death rate of 13%, and accounts for the second leading cancer death (Lacher and Hughes, 2015; Sonawane et al., 2016). The association of increased PCa risk with elevated expression of certain genes is indicated (Emami et al., 2019). Great efforts have been made for cancer prevention (Thompson et al., 2014), *in vivo* cancer probing (Liu et al., 2017a), and therapeutic intervention (Liu et al., 2017b). Nevertheless, early diagnosis and treatment are critical for curing PCa. Prostate-specific antigen (PSA) is currently considered as the most reliable serum biomarker for the diagnosis of PCa (Healy et al., 2007). Despite its wide application, PSA alone is not a cancer-specific biomarker because other non-cancerous prostate diseases, such as benign prostatic hyperplasia (BPH) and prostatitis can also induce the rising release of PSA into the circulation. The lack of specificity, particularly in the "diagnostic gray zone" of PSA values between 4 and 10 ng mL^{-1}, can induce to unnecessary prostate biopsies (Hoffman et al., 2000). In blood, PSA primarily binds to the serum protease inhibitor α1-antichymotrypsin (ACT) and forms a complex PSA-ACT (c-PSA), whereas a minor part appears as free PSA (f-PSA). The proportion of f-PSA in PCa is decreased, and the use of free-to-total PSA (f/t-PSA) ratio

* Corresponding author. Beijing Institute of Radiation Medicine, Beijing, 100850, PR China.
** Corresponding author. Beijing Institute of Radiation Medicine, Beijing, 100850, PR China.
*** Corresponding author. Beijing Institute of Radiation Medicine, Beijing, 100850, PR China.
E-mail addresses: wangchongwen1987@126.com (C. Wang), ruixiao203@sina.com (R. Xiao), sqwang@bmi.ac.cn (S. Wang).
[1] These authors contributed equally to this work.

https://doi.org/10.1016/j.bios.2019.111719
Received 9 September 2019; Accepted 19 September 2019
Available online 20 September 2019

in the serum can improve the specificity of PSA testing for PCa diagnosis (Catalona et al., 1998; Egawa et al., 1997; Jung et al., 2000). A cutoff value of 25% f/t-PSA ratio can detect 95% of cancers. Therefore, the simultaneous detection of f-PSA and c-PSA is critical to the PCa diagnostic accuracy for clinical samples with PSA values in the diagnostic gray zone.

Various analytical techniques, including surface-enhanced Raman scattering (SERS) immunoassay (Cheng et al., 2017; Gao et al., 2018), surface plasmon resonance immunoassay (Jiang et al., 2014), chemiluminescence enzyme immunoassay (Zhao et al., 2017), immuno fluorometric assay (Eriksson et al., 2000; Zhu et al., 2003), electrochemical sensor (Escamilla-Gómez et al., 2009), and chemiluminescence microarray immunoassay (Liu et al., 2016), have been developed for the simultaneous detection of f-PSA and c-PSA (or t-PSA) for PCa diagnosis. Nevertheless, most of these approaches require expensive laboratory instruments, skilled personnel, and time-consuming manual operation. These limitations have hindered their wide point-of-care detection applications, particularly in resource-limited settings, such as home, clinics, and infirmaries. Consequently, a simple, affordable, and easy-to-use diagnostic system with multiplex diagnostic capability is still urgently needed.

Lateral flow immunoassay (LFIA) is a rapid, affordable, and user-friendly point-of-care diagnostic technique for various bioanalysis applications. Two approaches are used to achieve multiplex detection based on the LFIA system. The first method is setting parallel test (T) lines or dots on nitrocellulose (NC) membrane with each T line for one analyte detection by using various kinds of report labels, including gold colloids (Brangel et al., 2018; Song et al., 2014), fluorescent nanoparticles (Song et al., 2015), upconversion nanoparticles (He et al., 2018; You et al., 2017), quantum dots (QDs) (Fang et al., 2018; Wu et al., 2016), and SERS tags (Wang et al. 2017, 2019). However, multiplex immunoassays for f-PSA and c-PSA detection usually share t-PSA antibody as the common capture antibody. Therefore, a multiplex detection approach based on parallel T lines is not capable of the duplex detection of f-PSA and c-PSA. Alternatively, the multiplex detection of analytes on a single T line has been reported based on multiplex report labels, such as multiple-color microspheres (Lee et al., 2016), and SERS tags (Noble et al., 2012; Tran et al., 2019; Zhang et al., 2018). However, colorimetric LFIA exhibits limited detection sensitivity and lacks quantitative diagnostics capability. The major drawbacks of SERS-based LFIAs are the relatively long readout time and their dependence on expensive Raman spectrometer for signal readout (Tran et al., 2019). Particularly, QDs-based fluorescent LFIA has been developed for the high sensitive detection of various analytes due to its distinguished optical features (Hu et al. 2016, 2017; Li et al., 2014; Qu et al., 2016). Different-sized QDs can be excited by using a single UV light source, and emit sharp and intensive fluorescence spectra with low crosstalk between the characteristic fluorescence peaks (Hu et al., 2010; Jennings et al., 2011; Wang et al., 2015b). As such, their multiplex encoding capacity for the simultaneous detection of several analytes was indicated.

Recently, magnetic-quantum dot nanobeads (MQBs), a kind of composite nanomaterial with distinct magnetic and fluorescent properties, have been employed as alternative probes for LFIA to improve the sensitivity and feasibility for analytes in complex biological metrix (Guo et al., 2019; Hu et al., 2019; Huang et al., 2019). Numerous QDs and magnetic nanobeads (MBs) were assembled or embedded into a single nanocomposite, thus yielding a substantially enhanced fluorescence signal. Moreover, specific antibody-conjugated MQBs can immune recognize, magnetically separate and enrich the analytes in complex samples under external magnetic field. Given the multiplex encoding capacity of QDs and analyte enrichment capability of MBs, the MQBs-based fluorescent LFIA possesses a considerable application potential for the high-sensitive and simultaneous detection of dual PSA markers on a single T line.

Herein, red and green MQBs with superior magnetic property and high luminescence were fabricated via polyethyleneimine (PEI)-mediated electrostatic adsorption of numerous QD625 or QD525 onto 140-nm-diameter superparamagnetic Fe_3O_4 magnetic cores. The synthesized dual-color MQBs were conjugated with f-PSA antibody and c-PSA antibody, respectively, as versatile fluorescent probes in test strip for immune recognition, magnetic enrichment, and simultaneous detection of f-PSA and c-PSA analytes in complex biological matrix. The t-PSA antibody was dispensed on a single T line as the common capture antibody. In the presence of f-PSA and c-PSA biomarkers in the sample, sandwich immunocomplexes would form on the T line through antibody−antigen reactions. A low-cost smartphone readout device, with some modifications to our previous work (Rong et al., 2019), was developed by integrating a 3D-printed smartphone attachment and optical and electrical components for dual-color fluorescent lateral flow strip imaging. A smartphone application was also created to facilitate image recording and data analysis. This LFIA platform achieved simultaneous point-of-care detection of f-PSA and c-PSA on a single T line with high specificity and sensitivity. Further, clinical serum samples of PCa and BPH patients were collected and evaluated to confirm the clinical feasibility of the proposed approach. To the best of our knowledge, MQBs-based fluorescent LFIA for simultaneous detection of dual biomarkers has not been reported. This work may provide new insights into the design and application of high-sensitive multiplex detection techniques for analytes in complex sample matrix.

2. Experimental section

2.1. Materials

Polyethyleneimine (PEI, MW 25 kDa), N-Hydroxysulfosuccinimide sodium salt (sulfo-NHS), 1-ethyl-3-(3-dimethylaminopropyl) carbodiimide·HCl (EDC), polyclonal goat anti-mouse IgG antibody, and bovine serum albumin (BSA) were purchased from Sigma-Aldrich. Carboxyl-functionalized CdSe/ZnS quantum dots (QD525 and QD625) were provided by Meso light Technology Corp. (Suzhou, China). Free prostate-specific antigen (f-PSA) was obtained from Lingchao Biotechnology Limited Company (Shanghai, China). Prostate-specific antigen-α1-antichymotrypsin complex (c-PSA), carcinoembryonic antigen (CEA), alpha-fetoprotein (AFP), carbohydrate antigen 19–9 (CA19-9), cancer antigen 125 (CA125), and cancer antigen 153 (CA153) were obtained from Fitzgerald Industries International, Inc. (Acton, MA, USA). Mouse monoclonal f-PSA, c-PSA, and total PSA (t-PSA) antibodies were obtained from BiosPacific, Inc. (CA, USA). Hi-Flow Plus 90 nitrocellulose (NC) membranes were obtained from Millipore (Billerica, MA, USA).

2.2. Preparation and antibody conjugation of MQBs

The superparamagnetic Fe_3O_4 magnetic nanobeads (MBs, 140 nm diameter) were synthesized through a solvothermal reaction (Wang et al., 2015a). Then, 0.1 g of prepared Fe_3O_4 MBs were mixed with PEI aqueous solution (5 mg mL^{-1}, 10 mL) under sonication for 30 min to self-assemble a positive-charged PEI layer on Fe_3O_4 MBs surface. After washing trice, Fe_3O_4@PEI MBs were mixed with carboxyl-functionalized QD525 or QD625 (10 μM, 50 μL), and sonicated for 30 min to form Fe_3O_4@PEI@QDs MQBs via electrostatic interactions.

Red-colored MQBs (MQB625) and green-colored MQBs (MQB525) were conjugated with f-PSA antibody and c-PSA antibody using carbodiimine chemistry, respectively. In brief, 500 μL of MQB625 or MQB525 suspension in MES solution (10 mM, pH 6.0) was mixed with EDC (10 mM, 10 μL) and sulfo-NHS (15 mM, 10 μL) at 37 °C for 15 min. After purification, carboxyl-activated MQBs were incubated with 15 μg of mouse monoclonal f-PSA antibody or c-PSA antibody for 1 h. Then, 25 μL of 1% BSA was added to block unreacted carboxyl sites. After purification again, MQB-antibody conjugates were resuspended in 200 μL of buffer solution for further use.

2.3. Preparation of lateral flow strips

The test line and control line were fabricated by spotting mouse monoclonal t-PSA antibody (0.8 mg mL^{-1}) and goat polyclonal anti-mouse IgG antibody (0.5 mg mL^{-1}) in coating buffer (10 mM PB, 3% methanol, pH 7.4) onto the NC membrane, respectively. Then, the plastic backing card assembled with the sample pad, NC membrane, and absorbent pad were cut into 3 mm wide lateral flow strips.

2.4. Simultaneous detection of f-PSA and c-PSA

A series of diluted f-PSA or c-PSA antigen solutions in 500 μL of buffer solution (10 mM PBS (pH 7.4), 0.05% Tween 20, and 25% fetal bovine serum) were prepared, and then incubated with f-PSA antibody-conjugated MQB625 (1 μL) and c-PSA antibody-conjugated MQB525 (1.5 μL) for 30 min. After magnetically separation and enrichment, immune complexes were resuspended in buffer solution (50 μL), and loaded onto the test strip for immune reaction of 20 min. The resulting strips were excited under UV light source and the fluorescence images were captured and analyzed by using the in-house created smartphone-based dual-color fluorescent lateral flow strip reader.

2.5. Analysis of clinical serum samples

Human serum samples of four PCa patients and four BPH patients were collected from the Department of Urology, Nanjing Jinling Hospital, and stored at −80 °C until use. Ethical approval for this research from the Research Ethics Committee of the hospital and informed consent documents from all these patients were obtained. Each clinical serum sample was tested by using the dual-color MQBs-based fluorescent LFIA platform. The values of f-PSA and c-PSA were simultaneously determined and compared with those determined by the chemiluminesent microparticle immunoassay (CMIA) system (Architect i2000SR, Abbott Laboratories, USA) at the hospital.

2.6. Smartphone-based dual-color fluorescent lateral flow strip reader

The smartphone readout device, with some modifications to our previous work (Rong et al., 2019), was developed to record the image of dual-color fluorescent lateral flow strips by integrating a smartphone (Mix2, Xiaomi) and optical and electrical components into a 3D-printed optomechanical attachment. A UV LED (3 W, 365 nm) was driven by a constant current driving circuit powered by two lithium batteries with a switch key. After being filtered by a 365 nm band-pass filter (Yongxing Optics, Beijing), UV light source was utilized to excite the MQBs probes captured on the test and control lines of LFIA strips with a 45° incidence angle. Fluorescence signals passed through a dual-band emission filter (524/628 nm, Edmund Optical, USA) to reduce background noise signals and crosstalk between red and green channels, and were collected by an external plano-convex lens (focal length: 20 mm, Edmund Optical, USA) before reaching the smartphone CMOS image sensor. For fluorescent lateral flow strip imaging, the optimal camera settings are an exposure time of 1/30 s and an ISO of 100. The smartphone application was designed by using Android Studio to facilitate image recording and data analysis. The application provides interfaces for users to input patient information, configure parameters, take strip images, and process data.

2.7. Characterization

Transmission electron microscopy (TEM) images of nanoparticles were taken using a Hitachi H-7650 TEM. Emission spectra were recorded by using a spectrometer (USB2000+, Ocean Optics, USA) under excitation of a handheld UV lamp. Zeta potentials were characterized by using a Nano-ZS90 Zeta Sizer (Malvern, UK). The magnetic properties were investigated using a superconducting quantum interference device magnetometer (SQUID, MPMSXL-7) at 300 K.

3. Results and discussion

3.1. Dual-color MQBs-Based fluorescent lateral flow immunoassay principle

In this work, the 140-nm-diameter superparamagnetic Fe_3O_4 MBs were synthesized through a solvothermal reaction, following the deposition of an ultrathin positive-charged PEI layer via self-assembly. Subsequently, numerous green- and red carboxyl-functionalized QDs were electrostatically adsorbed to form MQBs. Meanwhile, the as-synthesized MQB625 and MQB525 were conjugated with f-PSA antibody and c-PSA antibody, respectively, serving as the enrichment substrate as well as fluorescent probes in the LFIA (Fig. 1A). As shown in Fig. 1B, the as-synthesized Fe_3O_4 MBs are highly monodisperse nanospheres with a uniform diameter of ~140 nm. The positive-charged PEI mediate layer self-assembled as a bright ultrathin shell (~2 nm) surrounding the Fe_3O_4 cores in Fig. 1C for further electrostatic adsorption of negative-charged carboxylated QDs. Fig. 1D and E shows the as-synthesized MQB525 and MQB625 with numerous adsorbed QDs as small dots on the surface, which possess high luminescence and abundant carboxyl sites for antibody conjugation through amide reaction. The zeta potential increased from −27.7 mV of MBs to 42.5 mV of MB@PEI after self-assembly of positive-charged PEI layer, and then decreased to −4.76 mV of MQB525 and −6.62 mV of MQB625 because of numerous adsorbed carboxylated QDs (Fig. 1F). These results further confirm the successful preparation of MQBs. The magnetic property is critical to the separation efficiency and recovery of analytes. As shown in Fig. 1G, the magnetic hysteresis curves of MB, MB@PEI, MQB525 and MQB625 indicate their superior superparamagnetic property with a saturated magnetization of 66.1, 63.1, 54.5 and 55.9 emu g^{-1}, respectively. The decrease in magnetization is attributed to the less proportion of Fe_3O_4 in the as-synthesized nanocomposites (Guan et al., 2015). The magnetizations of as-synthesized MQBs are much stronger than that of recently reported similar nanocomposites (Guo et al., 2019; Hu et al., 2019; Huang et al., 2019), owing to the employment of superparamagnetic Fe_3O_4 magnetic cores and ultrathin PEI mediate layers in this work. The resultant MQB525 and MQB625 nanocomposites can be thoroughly enriched by using a magnetic bar in 30 s (Fig. S1). Furthermore, each MQB nanocomposite containing numerous QDs is expected to emit intensive fluorescence spectrum compared to a single QD (Guo et al., 2019). The photographs and fluorescence spectra of as-synthesized nanoparticles, and 1:1 mixture of MQB525 and MQB625 are shown in Fig. 1H and I. As expected, bright green and red optical emissions were observed for MQB525 and MQB625, respectively. As for their mixture, the fluorescent emission was yellow colored with two distinct peaks at 525 and 625 nm, and no obvious overlap was found between these two kinds of MQBs, indicating their great application potential for multiplex diagnostics technique with a low crosstalk between the different signal channels.

The analytical principle for simultaneous detection of dual PSA markers based on dual-color MQBs fluorescent probes is illustrated in Fig. 2. F-PSA antibody-conjugated MQB625, and c-PSA antibody-conjugated MQB525 would recognize, separate and enrich their responding antigens. After being loaded onto the lateral flow strips, the magnetic immunocomplexes migrated toward the absorption pad due to capillary effect and were captured by t-PSA antibody on the T line, forming sandwich immunocomplexes through antibody−antigen reactions. Under UV light, the T line of the strip used for f-PSA and c-PSA detection was red and green colored, respectively. Meanwhile, the resulting test line for their mixture was yellow colored as the merging of red and green fluorescent emissions. Thus, high-sensitive simultaneous point-of-care detection of dual PSA markers is expected based on the magnetic enrichment effect and dual-color high luminescence of the versatile MQBs probes in test strip.

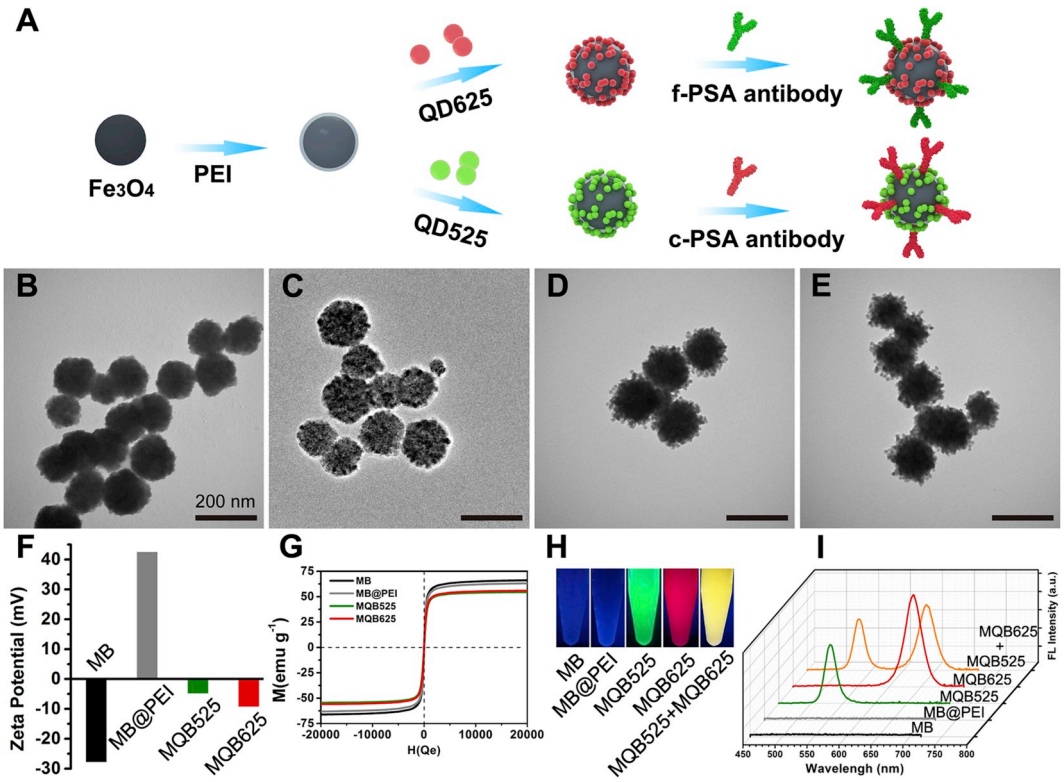

Fig. 1. Fabrication of dual-color MQBs fluorescent probes. (A) Schematic illustration of the synthesis process. TEM images of (B) MB, (C) MB@PEI, (D) MQB525, and (E) MQB625, and their (F) zeta potentials, (G) magnetic hysteresis curves, (H) photographs and (I) fluorescence spectra under UV light. (For interpretation of the references to color in this figure legend, the reader is referred to the Web version of this article.)

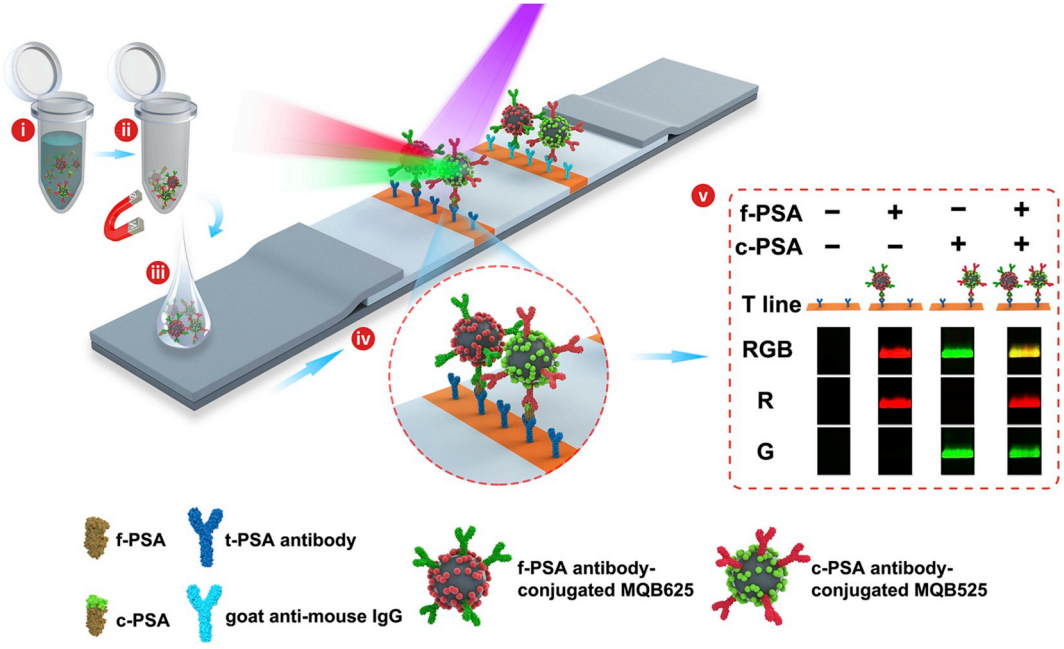

Fig. 2. Schematic illustration of the dual-color MQBs-based fluorescent LFIA. (i) Mixing of f-PSA, c-PSA, f-PSA antibody-conjugated MQB625, and c-PSA antibody-conjugated MQB525. (ii) Magnetic separation and enrichment of dual PSAs. (iii) Loading magnetic immunocomplexes onto the lateral flow test strips. (iv) Simultaneous capture of immunocomplexes by t-PSA antibody on the T line. (v) Imaging and interpretation of results. (For interpretation of the references to color in this figure legend, the reader is referred to the Web version of this article.)

As portable wireless communication devices, smartphones are integrated with high-performance digital camera and computational processing power that allows for the miniaturization of the optical readout device for point-of-care diagnostics applications (Ding et al., 2019; Draz et al., 2018; Joung et al., 2019; Kong et al., 2017; Min et al., 2018). Despite current great efforts (Brangel et al., 2018; He et al., 2018; Michelini et al., 2019; Rong et al., 2019; You et al., 2017; Zhao et al., 2018), the optimal optical design and data processing algorithm of

smartphone-based reader for dual-color fluorescent test strip remain challenging. In this study, a 3D-printed smartphone attachment was employed to integrate a smartphone (Mix2, Xiaomi) and optical and electrical components for the dual-color imaging of the fluorescent lateral flow strip. The sharp and size-tunable fluorescent emission spectra of QDs can be excited by a single UV light source, regardless of their different emission wavelengths. Therefore, the simplified and compact optical design with a single 365 nm UV light excitation source for both MQB625 and MQB525 was enabled as shown in Fig. 3A. As a contrast, multiplex imaging analysis based on traditional organic fluorescent dyes requires separate excitation light sources, filters, and optical paths (Awqatty et al., 2014; Kuhnemund et al., 2017). In particular, a dual-band emission filter was employed in this work to reduce the background noise signals and crosstalk between red and green signal channels. An external plano-convex lens fixed in front of the smartphone CMOS image sensor allows for signal collection and image magnification, and the object distance was reduced to 20 mm that enables the miniaturization of the smartphone readout device with an overall dimension of ~160 mm × 80 mm × 40 mm (Fig. 3B). The optical and electrical components of the proposed dual-color strip reader cost approximately $250.

A smartphone application was custom-designed to facilitate the device control and data processing. This application provides interfaces for users to input patient information, configure parameters, take test strip photos, and process data (Fig. S2). The application can simultaneously calculate the values of f-PSA and c-PSA following the image processing procedure as described in Fig. S3. Red and green fluorescence signals emitting from the dual-color MQBs probes were captured by the smartphone RGB CMOS sensor in the proposed reader. A 300 × 350 rectangular region covering the test line was selected in the obtained RGB image, which was subsequently split into R, G and B channels. For R or G channels, each signal peak area and baseline signal were calculated, and background-subtracted average value was regarded as the R or G channel intensity. The calibration curves for f-PSA and c-PSA were obtained via the sigmoidal curve fitting of the calculated R and G channel intensities of standard analytes, respectively. The fitting parameters were fed to the parameter configuring menu of the application for the following calculation of f-PSA and c-PSA concentrations of the clinical samples.

3.2. Assay development

The fluorescent emission of MQB625 was more intensive than that of MQB525 due to their different quantum yields. Given the minor proportion of f-PSA existing in blood, MQB625 and MQB525 were conjugated with f-PSA antibody and c-PSA antibody, respectively. Meanwhile, the volume of c-PSA antibody-conjugated MQB525 (1.5 μL) for preparation of the conjugate pad was higher than that of f-PSA antibody-conjugated MQB625 (1 μL) to balance the optical emissions of red and green fluorescent signals. In this assay, MQBs with a magnetic core size of 140 nm and 200 nm were synthesized to evaluate its effect on assay performance. As shown in Fig. S4, MQBs with a core diameter of 140 nm exhibited a stronger fluorescence intensity on the test line, which is attributed to the high surface-to-volume ratio to facilitate immune reaction efficiency. Furthermore, the relative-small diameter size with sufficient magnetic property was selected in this assay to avoid potential steric hindrance and non-specific adsorption when the magnetic immunocomplexes immigrated through the NC membrane. The detection antibody amount was optimized to improve the analytical performance of the dual-color LFIA. The optimal detection antibody amounts for f-PSA antibody and c-PSA antibody were both 15 μg for antibody conjugation to 500 μL of MQBs based on the test line intensities for the resulting test strips of 1 ng mL^{-1} of f-PSA (red channel intensity) and 5 ng mL^{-1} of c-PSA (green channel intensity), respectively (Fig. S5).

Dual-color MQBs-based fluorescent LFIA for f-PSA and c-PSA detection separately was performed to verify the feasibility of the assay. A series of diluted f-PSA and c-PSA solutions in the range 0.01–100 ng mL^{-1} were allowed to mix and immune bind with antibody-conjugated MQBs probes for 30 min. The resulting immunocomplexes were collected under the external magnetic field to separate and enrich analytes from complex sample matrix. Then, the concentrated immunocomplexes were loaded onto the test strips and finally immobilized by t-PSA antibody on the test line, which were further excited by UV light and captured by the smartphone readout device. The analyte enrichment ability of MQBs probes were also confirmed (Fig. S6). Images of the test strips with red test line for f-PSA detection (Fig. 4A) and green test line for c-PSA detection (Fig. 4B) can be observed. The red and green fluorescent intensities were well fitted by sigmoidal curves (Fig. 4C and D). The red or green test line of the test strip became brighter with the increasing concentration of f-PSA or c-PSA in the sample. The test lines corresponding to 0.05 ng mL^{-1} of f-PSA and 0.5 ng mL^{-1} of c-PSA can be observed by the naked eye. This

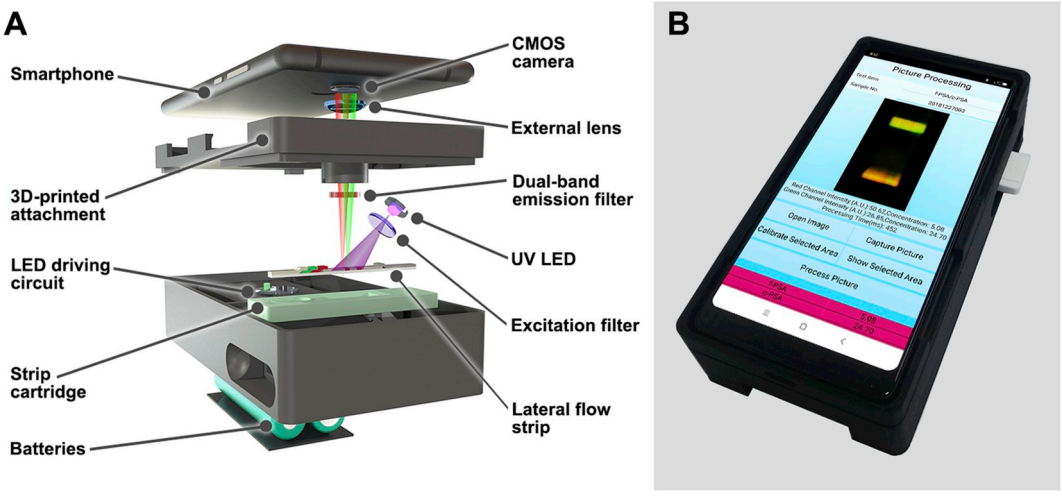

Fig. 3. Smartphone-based dual-color fluorescent lateral flow strip reader. (A) Internal structure of the smartphone readout device. MQB625 and MQB525 conjugates captured on the test line were excited by a 365 nm UV LED light source. Red and green emission signals passed through a dual-band emission filter (524/628 nm) and an external plano-convex lens, before reaching the smartphone CMOS sensor. (B) Image of the smartphone readout device. (For interpretation of the references to color in this figure legend, the reader is referred to the Web version of this article.)

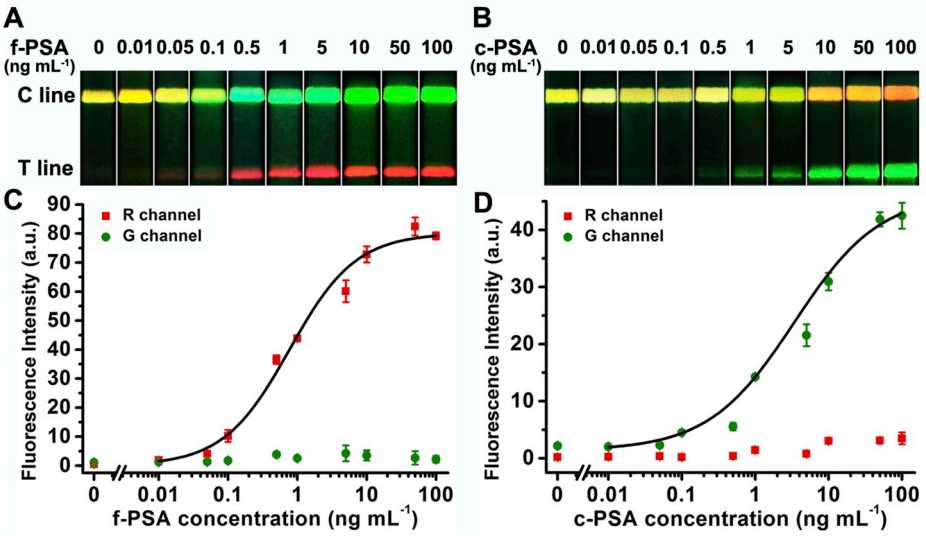

Fig. 4. Analytical performance of dual-color fluorescent LFIA. Images of the test strips at different concentrations of (A) f-PSA (0.01–100 ng mL^{-1}) and (B) c-PSA (0.01–100 ng mL^{-1}). Corresponding test line intensities of red channel (red square) and green channel (green dot) and calibration curves for (C) f-PSA and (D) c-PSA. Error bars represent the standard deviation of three repetitive experiments. (For interpretation of the references to color in this figure legend, the reader is referred to the Web version of this article.)

difference between the signal responses is mainly attributed to the stronger quantum yield of red-color QD625 than that of green-color QD525 and the difference in immunity affinity between the immunoassays for f-PSA and c-PSA. The background signal arising from the nonspecific adsorption of MQBs probes and the crosstalk between red and green signal channels are critical for multiplex diagnostics method. In this work, the as-synthesized MQBs possess excellent monodispersity with a small diameter (<170 nm), thus leading to a low background signal level. Furthermore, the possible crosstalk can be hindered by the narrow distinct fluorescent emissions of MQBs and the employment of dual-band emission filter. Taken together, relatively low background and crosstalk signals were demonstrated in Fig. 4C and D. The calibration curves of the red fluorescence for f-PSA detection and the green fluorescence for c-PSA detection exhibited a sigmoidal function of f-PSA and c-PSA value in the range of 0.01–100 ng mL^{-1}, respectively. The limits of detection (LODs), estimated from the sigmoidal fitting curve where the analyte concentration generates the signal intensity value that exceeds three times the standard deviation (SD) of the blank measurements, are 0.008 ng mL^{-1} of f-PSA and 0.061 ng mL^{-1} of c-PSA. This calculation is reasonable because the invisible fluorescent signals for the naked eyes can be analyzed by the processing algorithm to generate a lower LOD value.

The specificity of this assay was investigated by using several cancer biomarkers, including CEA (100 ng mL^{-1}), AFP (100 ng mL^{-1}), CA19-9 (1 kU mL^{-1}), CA125 (1 kU mL^{-1}), and CA153 (100 U mL^{-1}), as the interferents. These cancer biomarkers and blank control exhibited a relatively low signal in both red and green channels, whereas f-PSA (1 ng mL^{-1}) or c-PSA (5 ng mL^{-1}) exhibited a distinct signal in red channel and green channel, respectively (Fig. S7). The results indicate the high specificity of the dual-color LFIA toward the target analytes.

3.3. Simultaneous detection of f-PSA and c-PSA

The cross reaction between immunoassays for different analytes is another critical factor for a multiplex diagnostics method. A total of 10 ng mL^{-1} of t-PSA solutions with different concentration ratios of f-PSA and c-PSA were tested by using the proposed dual-color LFIA to evaluate the cross reactivity between f-PSA and c-PSA antigens. As shown in Fig. 5A, the test line of the test strip turned from green to red as the concentration of c-PSA was decreased and that of f-PSA was increased. The red and green channel intensities were readout as shown in Fig. 5B to characterize f-PSA and c-PSA, respectively. This result further confirmed the color trend of the test lines as expected. In addition, the dual-color readout values were constant with those for only one

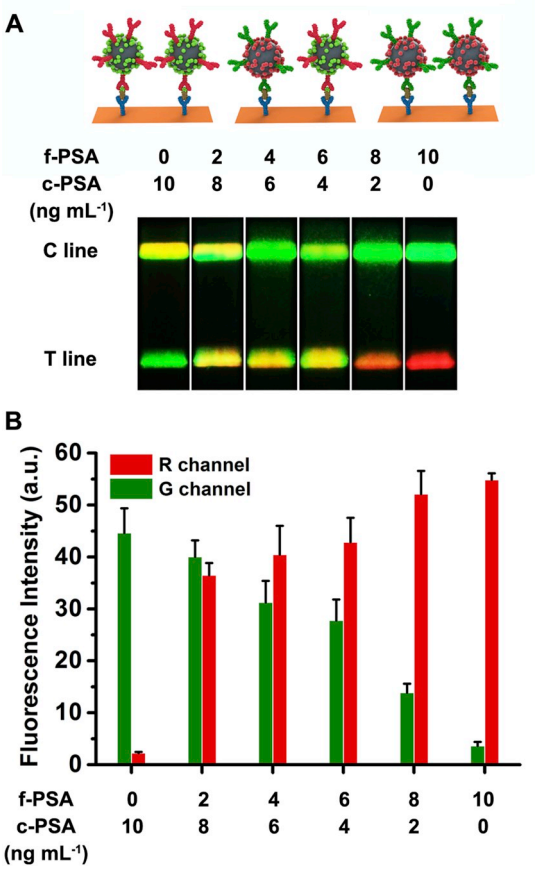

Fig. 5. (A) Images of the test strips and (B) corresponding test line intensities at different concentration ratios of f-PSA and c-PSA. Error bars represent the standard deviation of three repetitive experiments.

kind of PSA antigen in the samples as shown in Fig. 4C and D. These results indicate that the red and green channel readouts depended on the corresponding concentration of f-PSA and c-PSA in the sample, and a negligible cross activity between these two PSA biomarkers exists. Thus, simultaneous detection of f-PSA and c-PSA on a single T line is feasible based on the multiplexing capability of the proposed LFIA platform.

Various concentrations of f-PSA (0.05–20 ng mL^{-1}) and c-PSA

(0.2–80 ng mL^{-1}) with a 1:4 concentration ratio were spiked into FBS used to simulate the human serum matrixes, followed by testing using the dual-color lateral flow strips to verify the duplex detection capability of the proposed LFIA platform. The test strip images were captured (Fig. 6A), and the orange-yellow color as observed on the test lines became brighter with the increasing concentrations of f-PSA and c-PSA. Their corresponding red and green channel intensities were readout by the smartphone reader as shown in Fig. 6B, which increased with the increase in f-PSA and c-PSA concentrations, respectively. Corresponding calibration curves for f-PSA and c-PSA are shown in Fig. 6C and D. Subsequently, the fitting parameters were fed back to the parameter configuring menu of the application for the following simultaneous calculation of f-PSA and c-PSA concentrations of clinical serum samples. The LODs were calculated to be 0.009 ng mL^{-1} of f-PSA and 0.087 ng mL^{-1} of c-PSA, which are acceptable for clinical diagnostics because the cutoff concentration of t-PSA is 4.0 ng mL^{-1}. As summarized in Table S1 in the Supporting Information, the proposed MQBs-based fluorescent LFIA shows superior analytical sensitivity for the simultaneous detection of dual PSA markers. The reproducibility of dual-color fluorescent LFIA for simultaneous detection of f-PSA and c-PSA is shown in Fig. S8. The relative standard deviations for different concentrations of f-PSA and c-PSA are indicated as acceptable. Furthermore, the as-prepared antibody-conjugated MQBs probes and test strips were lyophilized and then stored for 4 weeks at room temperature. A good stability of the proposed assay is shown in Fig. S9, indicating its wide application capability in low-resource settings.

3.4. Application in clinical samples

To investigate the clinical feasibility of the proposed method, recovery experiments were performed by testing f-PSA and c-PSA analytes spiked into two human serum samples. As shown in Table S2, the recoveries of f-PSA and c-PSA in human samples range from 91.00% to 108.00%. Furthermore, f-PSA and c-PSA values in clinical serum samples were tested by this platform. Human serum samples of four PCa patients and four BPH patients were collected from the hospital. The simultaneously determined f-PSA and c-PSA values were compared with results determined by using the CMIA system in Table S3. The results obtained from the dual-color fluorescent LFIA platform are consistent with those obtained from the CMIA system. The mean values of measured f/t-PSA ratios for BPH and PCa are 0.28 and 0.12, respectively, which are close to previously reported values (Jiang et al., 2014; Jung et al., 2000). Therefore, the proposed dual-color MQBs-based fluorescent LFIA platform possesses the capability of simultaneous point-of-care detection of f-PSA and c-PSA in clinical serum samples and could greatly facilitate the accurate diagnosis of PCa in the clinical practice.

4. Conclusions

In this study, we demonstrated the simultaneous point-of-care detection of dual PSA markers in clinical samples for accurate diagnosis of PCa using MQBs-based fluorescent lateral flow test strip. Red and green MQBs were fabricated via PEI-mediated electrostatic adsorption of numerous QD525 or QD625 onto superparamagnetic Fe_3O_4 magnetic cores. The synthesized red and green MQBs possess excellent monodispersity, superior magnetic property and high luminescence, and were conjugated with f-PSA antibody and c-PSA antibody, respectively, as versatile fluorescent probes for immune recognition, magnetic enrichment, and simultaneous detection of f-PSA and c-PSA analytes in complex biological matrix. A relatively low crosstalk and cross-reactivity between the immunoassays for dual PSA markers were demonstrated. This assay is capable of the simultaneous detection of f-PSA and c-PSA with LODs of 0.009 ng mL^{-1} and 0.087 ng mL^{-1}, respectively, in a short assay time of 60 min. Clinical serum samples of PCa and BPH patients were collected and evaluated by using the proposed approach. The obtained results were consistent with reference values, indicating the clinical feasibility of this diagnostics technique for testing PSA markers in the diagnostic gray zone. Given its easy-to-use format, duplex detection capacity, and superior analytical performance, the proposed dual-color MQBs-based fluorescent LFIA is a promising point-of-care diagnostics technique for the accurate diagnosis of PCa even in resource-limited settings.

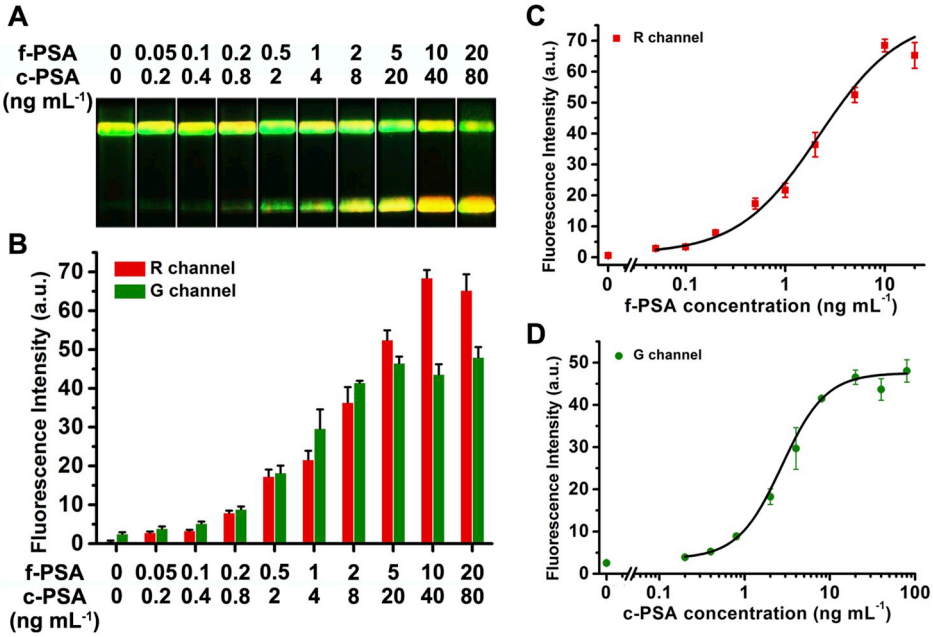

Fig. 6. Simultaneous detection of f-PSA and c-PSA. (A) Images of the test strips and (B) corresponding test line intensities for simultaneous detection of a 1:4 concentration ratio mixture of f-PSA (0.05–20 ng mL^{-1}) and c-PSA (0.2–80 ng mL^{-1}). Corresponding calibration curves for (C) f-PSA and (D) c-PSA. Error bars represent the standard deviation of three repetitive experiments.

Declaration of competing interest

The authors declare that they have no known competing financial interests or personal relationships that could have appeared to influence the work reported in this paper.

CRediT authorship contribution statement

Zhen Rong: Methodology, Writing - original draft. **Zikun Bai:** Methodology, Writing - original draft. **Jianing Li:** Software, Writing - original draft. **Hao Tang:** Methodology. **Tianyi Shen:** Methodology. **Qiong Wang:** Methodology. **Chongwen Wang:** Methodology, Writing - review & editing, Supervision. **Rui Xiao:** Writing - review & editing, Supervision. **Shengqi Wang:** Writing - review & editing, Supervision.

Acknowledgements

Z.R., Z.K.B. and J.N.L. contributed equally to this work. This study was supported by the National Natural Science Foundation of China (Grant no. 81902159), the National S&T Major Project for Infectious Diseases Control (2018ZX10712001-010, 2018ZX10101003-001), the Natural Science Foundation of Anhui Province (Grant no. 1908085QB85), and the Natural Foundation of Jiangsu Province (Grant no. BK20140735). J.N.L., an intern student of Beijing Institute of Radiation Medicine, is from Beijing National Day School.

Appendix A. Supplementary data

Supplementary data to this article can be found online at https://doi.org/10.1016/j.bios.2019.111719.

References

Awqatty, B., Samaddar, S., Cash, K.J., Clark, H.A., Dubach, J.M., 2014. Analyst 139, 5230–5238.
Brangel, P., Sobarzo, A., Parolo, C., Miller, B.S., Howes, P.D., Gelkop, S., Lutwama, J.J., Dye, J.M., McKendry, R.A., Lobel, L., Stevens, M.M., 2018. ACS Nano 12, 63–73.
Catalona, W.J., Partin, A.W., Slawin, K.M., et al., 1998. J. Am. Med. Assoc. 279, 1542–1547.
Cheng, Z., Choi, N., Wang, R., Lee, S., Moon, K.C., Yoon, S.Y., Chen, L., Choo, J., 2017. ACS Nano 11, 4926–4933.
Ding, X., Mauk, M.G., Yin, K., Kadimisetty, K., Liu, C., 2019. Anal. Chem. 91, 655–672.
Draz, M.S., Kochehbyoki, K.M., Vasan, A., Battalapalli, D., Sreeram, A., Kanakasabapathy, M.K., Kallakuri, S., Tsibris, A., Kuritzkes, D.R., Shafiee, H., 2018. Nat. Commun. 9, 4282.
Egawa, S., Soh, S., Ohori, M., Uchida, T., Gohji, K., Fujii, A., Kuwao, S., Koshiba, K., 1997. Cancer 79, 90–98.
Emami, N.C., Kachuri, L., Meyers, T.J., Das, R., Hoffman, J.D., Hoffmann, T.J., Hu, D., Shan, J., Feng, F.Y., Ziv, E., Van Den Eeden, S.K., Witte, J.S., 2019. Nat. Commun. 10, 3107.
Eriksson, S., Vehniainen, M., Jansen, T., Meretoja, V., Saviranta, P., Pettersson, K., Lovgren, T., 2000. Clin. Chem. 46, 658–666.
Escamilla-Gómez, V., Hernández-Santos, D., González-García, M.B., Pingarrón-Carrazón, J.M., Costa-García, A., 2009. Biosens. Bioelectron. 24, 2678–2683.
Fang, C.C., Chou, C.C., Yang, Y.Q., Wei-Kai, T., Wang, Y.T., Chan, Y.H., 2018. Anal. Chem. 90, 2134–2140.
Gao, R., Cheng, Z., Wang, X., Yu, L., Guo, Z., Zhao, G., Choo, J., 2018. Biosens. Bioelectron. 119, 126–133.
Guan, X., Chang, J., Chen, Y., Fan, H., 2015. RSC Adv. 5, 50126–50136.
Guo, L., Shao, Y., Duan, H., Ma, W., Leng, Y., Huang, X., Xiong, Y., 2019. Anal. Chem. 91, 4727–4734.
He, H., Liu, B., Wen, S., Liao, J., Lin, G., Zhou, J., Jin, D., 2018. Anal. Chem. 90, 12356–12360.
Healy, D.A., Hayes, C.J., Leonard, P., McKenna, L., O'Kennedy, R., 2007. Trends Biotechnol. 25, 125–131.
Hoffman, R.M., Clanon, D.L., Littenberg, B., Frank, J.J., Peirce, J.C., 2000. J. Gen. Intern. Med. 15, 739–748.
Hu, J., Jiang, Y.-Z., Tang, M., Wu, L.-L., Xie, H.-y., Zhang, Z.-L., Pang, D.-W., 2019. Anal. Chem. 91, 1178–1184.
Hu, J., Jiang, Y.-Z., Wu, L.-L., Wu, Z., Bi, Y., Wong, G., Qiu, X., Chen, J., Pang, D.-W., Zhang, Z.-L., 2017. Anal. Chem. 89, 13105–13111.
Hu, J., Zhang, Z.-L., Wen, C.-Y., Tang, M., Wu, L.-L., Liu, C., Zhu, L., Pang, D.-W., 2016. Anal. Chem. 88, 6577–6584.
Hu, M., Yan, J., He, Y., Lu, H., Weng, L., Song, S., Fan, C., Wang, L., 2010. ACS Nano 4, 488–494.
Huang, Z., Peng, J., Han, J., Zhang, G., Huang, Y., Duan, M., Liu, D., Xiong, Y., Xia, S., Lai, W., 2019. Food Chem. 276, 333–341.
Jennings, T.L., Becker-Catania, S.G., Triulzi, R.C., Tao, G., Scott, B., Sapsford, K.E., Spindel, S., Oh, E., Jain, V., Delehanty, J.B., Prasuhn, D.E., Boeneman, K., Algar, W. R., Medintz, I.L., 2011. ACS Nano 5, 5579–5593.
Jiang, Z., Qin, Y., Peng, Z., Chen, S., Chen, S., Deng, C., Xiang, J., 2014. Biosens. Bioelectron. 62, 268–273.
Joung, H.-A., Ballard, Z.S., Ma, A., Tseng, D.K., Teshome, H., Burakowski, S., Garner, O. B., Di Carlo, D., Ozcan, A., 2019. Lab Chip 19, 1027–1034.
Jung, K., Elgeti, U., Lein, M., Brux, B., Sinha, P., Rudolph, B., Hauptmann, S., Schnorr, D., Loening, S.A., 2000. Clin. Chem. 46, 55–62.
Kong, J.E., Wei, Q., Tseng, D., Zhang, J., Pan, E., Lewinski, M., Garner, O.B., Ozcan, A., Di Carlo, D., 2017. ACS Nano 11, 2934–2943.
Kuhnemund, M., Wei, Q., Darai, E., Wang, Y., Hernandez-Neuta, I., Yang, Z., Tseng, D., Ahlford, A., Mathot, L., Sjoblom, T., Ozcan, A., Nilsson, M., 2017. Nat. Commun. 8, 13913.
Lacher, D.A., Hughes, J.P., 2015. Clin. Chim. Acta 448, 220–227.
Lee, S., Mehta, S., Erickson, D., 2016. Anal. Chem. 88, 8359–8363.
Li, X., Li, W., Yang, Q., Gong, X., Guo, W., Dong, C., Liu, J., Xuan, L., Chang, J., 2014. ACS Appl. Mater. Interfaces 6, 6406–6414.
Liu, A., Zhao, F., Zhao, Y., Shangguan, L., Liu, S., 2016. Biosens. Bioelectron. 81, 97–102.
Liu, C., Yang, C., Lu, L., Wang, W., Tan, W., Leung, C.H., Ma, D.L., 2017. Chem. Commun. 53, 2822–2825.
Liu, L.J., Wang, W., Huang, S.Y., Hong, Y., Li, G., Lin, S., Tian, J., Cai, Z., Wang, H.D., Ma, D.L., Leung, C.H., 2017. Chem. Sci. 8, 4756–4763.
Michelini, E., Calabretta, M.M., Cevenini, L., Lopreside, A., Southworth, T., Fontaine, D. M., Simoni, P., Branchini, B.R., Roda, A., 2019. Biosens. Bioelectron. 123, 269–277.
Min, J., Nothing, M., Coble, B., Zheng, H., Park, J., Im, H., Weber, G.F., Castro, C.M., Swirski, F.K., Weissleder, R., Lee, H., 2018. ACS Nano 12, 3378–3384.
Noble, J., Attree, S., Horgan, A., Knight, A., Kumarswami, N., Porter, R., Worsley, G., 2012. Anal. Chem. 84, 8246–8252.
Qu, H., Zhang, Y., Qu, B., Kong, H., Qin, G., Liu, S., Cheng, J., Wang, Q., Zhao, Y., 2016. Biosens. Bioelectron. 81, 358–362.
Rong, Z., Wang, Q., Sun, N., Jia, X., Wang, K., Xiao, R., Wang, S., 2019. Anal. Chim. Acta 1055, 140–147.
Sonawane, M.D., Nimse, S.B., Song, K.-S., Kim, T., 2016. RSC Adv. 6, 7599–7609.
Song, L.W., Wang, Y.B., Fang, L.L., Wu, Y., Yang, L., Chen, J.Y., Ge, S.X., Zhang, J., Xiong, Y.Z., Deng, X.M., Min, X.P., Zhang, J., Chen, P.J., Yuan, Q., Xia, N.S., 2015. Anal. Chem. 87, 5173–5180.
Song, S., Liu, N., Zhao, Z., Njumbe Ediage, E., Wu, S., Sun, C., De Saeger, S., Wu, A., 2014. Anal. Chem. 86, 4995–5001.
Thompson Jr., I.M., Cabang, A.B., Wargovich, M.J., 2014. Nat. Rev. Clin. Oncol. 11, 49–60.
Tran, V., Walkenfort, B., König, M., Salehi, M., Schlücker, S., 2019. Angew. Chem. Int. Ed. 58, 442–446.
Wang, C., Wang, C., Wang, X., Wang, K., Zhu, Y., Rong, Z., Wang, W., Xiao, R., Wang, S., 2019. ACS Appl. Mater. Interfaces 11, 19495–19505.
Wang, C., Xu, J., Wang, J., Rong, Z., Li, P., Xiao, R., Wang, S., 2015. J. Mater. Chem. C 3, 8684–8693.
Wang, J.-J., Jiang, Y.-Z., Lin, Y., Wen, L., Lv, C., Zhang, Z.-L., Chen, G., Pang, D.-W., 2015. Anal. Chem. 87, 11105–11112.
Wang, X., Choi, N., Cheng, Z., Ko, J., Chen, L., Choo, J., 2017. Anal. Chem. 89, 1163–1169.
Wu, F., Yuan, H., Zhou, C., Mao, M., Liu, Q., Shen, H., Cen, Y., Qin, Z., Ma, L., Song Li, L., 2016. Biosens. Bioelectron. 77, 464–470.
You, M., Lin, M., Gong, Y., Wang, S., Li, A., Ji, L., Zhao, H., Ling, K., Wen, T., Huang, Y., Gao, D., Ma, Q., Wang, T., Ma, A., Li, X., Xu, F., 2017. ACS Nano 11, 6261–6270.
Zhang, D., Huang, L., Liu, B., Su, E., Chen, H.-Y., Gu, Z., Zhao, X., 2018. Sens. Actuators B Chem. 277, 502–509.
Zhao, L., Wang, D., Shi, G., Lin, L., 2017. Luminescence 32, 1547–1553.
Zhao, Y., Yang, M., Fu, Q., Ouyang, H., Wen, W., Song, Y., Zhu, C., Lin, Y., Du, D., 2018. Anal. Chem. 90, 7391–7398.
Zhu, L., Leinonen, J., Zhang, W.M., Finne, P., Stenman, U.H., 2003. Clin. Chem. 49, 97–103.